

Random matrix model for QCD₃ staggered fermions

P. Bialas^{1,2,*}, Z. Burda^{1,2,†} and B. Petersson^{3,4‡}

¹*Marian Smoluchowski Institute of Physics, Jagiellonian University, Reymonta 4, 30-059 Kraków, Poland*

²*Mark Kac Complex Systems Research Centre, Jagiellonian University, Reymonta 4, 30-059 Kraków, Poland*

³*Faculty of Physics, University of Bielefeld, P.O. Box 10 01 21, D-33501 Bielefeld, Germany*

⁴*Institute of Physics, Humboldt University, Newtonstr. 15, D-12489 Berlin, Germany*

We show that the lowest part of the eigenvalue density of the staggered fermion operator in lattice QCD₃ at small lattice coupling constant β has exactly the same shape as in QCD₄. This observation is quite surprising, since universal properties of the QCD₃ Dirac operator are expected to be described by a non-chiral matrix model. We show that this effect is related to the specific nature of the staggered fermion discretization and that the eigenvalue density evolves towards the non-chiral random matrix prediction when β is increased and the continuum limit is approached. We propose a two-matrix model with one free parameter which interpolates between the two limits and very well mimics the pattern of evolution with β of the eigenvalue density of the staggered fermion operator in QCD₃.

Introduction

One can argue, referring to the universality [1], that the low energy properties of the QCD₄ Dirac operator in the ϵ -regime are described by the chiral random matrix model [2]. In particular, the microscopic eigenvalue density of the Dirac operator, which is obtained from the eigenvalue density

$$\rho(\lambda) = \left\langle \sum_i \delta(\lambda - \lambda_i) \right\rangle \quad (1)$$

by blowing it up at $\lambda = 0$, is expected to have the same universal shape as in the random matrix. More precisely, the microscopic eigenvalue density is defined as

$$\rho_*(\lambda) = \lim_{N \rightarrow \infty} \frac{1}{N\Sigma} \rho\left(\frac{\lambda}{N\Sigma}\right), \quad (2)$$

where $\Sigma = \pi\rho(0)$ and N is the number of eigenvalues' pairs of the underlying discretized (regularized) Dirac operator, N is related to the physical volume $V \sim Na^D$ where a is an UV-cut-off. The microscopic density $\rho_*(\lambda)$ can be determined analytically using the random matrix model. For the trivial topological sector and for $N_f = 0$ flavors it reads [2]

$$\rho_{4*}(\lambda) = \frac{\lambda}{2} (J_0^2(\lambda) + J_1^2(\lambda)). \quad (3)$$

This eigenvalue density has been compared to numerical data from quenched Monte-Carlo simulations of lattice QCD with staggered fermions [3]. One could indeed see a very good agreement between the random matrix prediction and lattice data [4]. It has later been shown that with an improved staggered action also the non trivial topological sectors are well described [5].

If one applies the same arguments to QCD₃ one is led to a non-chiral random matrix model and to the following microscopic density [6]

$$\rho_{3*}(\lambda) = \frac{1}{\pi}. \quad (4)$$

Also this prediction can be easily tested numerically by comparing it to lattice QCD₃ data. Actually some tests have been done in the past but they were not conclusive [7]. In this work we repeat quenched simulations of lattice QCD₃

*pbialas@th.if.uj.edu.pl

†zdzislaw.burda@uj.edu.pl

‡bengt@physik.hu-berlin.de

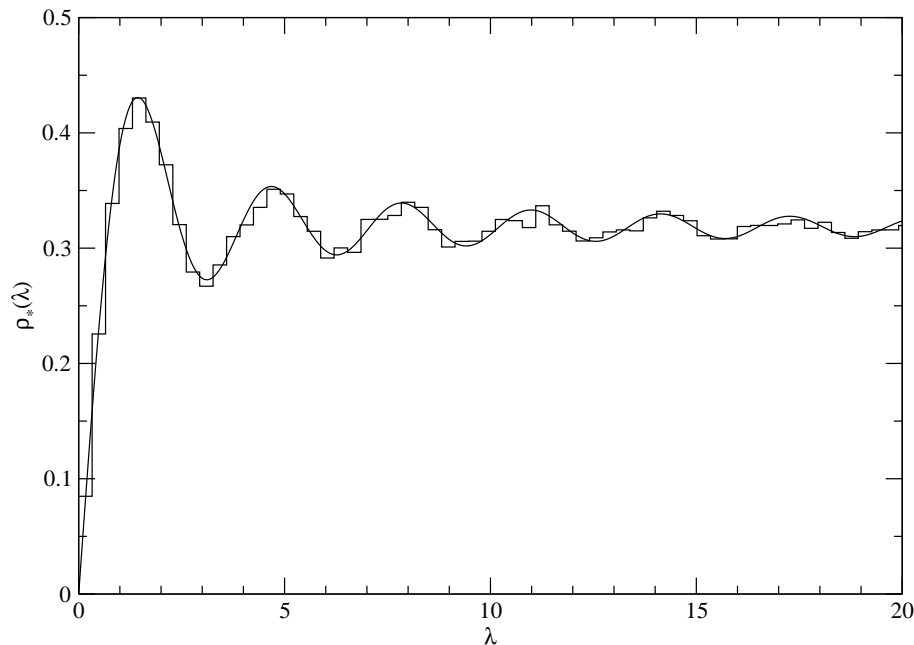


FIG. 1: Comparison of the lowest part of the eigenvalue distribution of the staggered fermion operator obtained in Monte-Carlo simulations of quenched QCD₃ with the $SU(3)$ Wilson action for $\beta = 6$ on a 14^3 lattice to the chiral random matrix prediction (blue dotted line) and the corresponding non-chiral random matrix prediction (green solid line). The data fits perfectly to the chiral random matrix density.

to determine the eigenvalue density of the staggered fermion operator. The spectrum of the lowest positive eigenvalues of the staggered fermion operator for quenched QCD₃ with $\beta = 6.0$ is shown in figure 1. As one can see the result is quite surprising. The QCD₃ data matches the chiral prediction (3) and not the non-chiral one (4) anticipated in this case. This finding raises the following questions for discussion. Why a three dimensional theory which has no chiral symmetry shows a pattern characteristic for a chiral theory? Is the effect related to the regularization scheme? If yes, will it disappear when the continuum limit is approached? In QCD₄ where the chiral symmetry plays an important role, the pattern will stay intact when β is increased and the continuum limit is approached while in QCD₃ the shape of the lowest part of the spectrum should gradually evolve from (3) to (4). These questions will be addressed in the remaining part of the paper. The paper is organized as follows. In the next section we recall the matrix models used to describe the universal properties of the lowest part of the Dirac operator spectrum in four and three dimensions. We emphasize the difference between them. Then we discuss staggered fermions and introduce a new matrix model with one free parameter to imitate the evolution with β of the staggered fermion operator spectra in QCD₃. It describes a gradual disappearance of a hard edge at the origin of the spectrum when β goes to infinity. We compare the low energy part of the eigenvalue distribution of quenched QCD₃ and of the random matrix model. We conclude the paper with a short summary.

Random matrix model

The relation of the low energy spectrum of the Dirac operator in four dimensions to the chiral random matrix model has been extensively discussed in the literature so here we will restrict ourselves to a minimal presentation which is concentrated on the difference between the chiral and the non-chiral case. The interested reader is referred to reviews [8, 9] and the references therein. In four dimensions the Euclidean Dirac operator assumes in the chiral representation the following form

$$\mathcal{D} = \begin{pmatrix} 0 & i\mathcal{W}^\dagger \\ i\mathcal{W} & 0 \end{pmatrix} \quad (5)$$

where

$$\mathcal{W} = \mathcal{W}_4 \mathbb{1} + i \sum_{k=1}^3 \mathcal{W}_k \sigma_k , \quad (6)$$

$\mathbb{1}$ is a 2×2 unit matrix, σ_k , $k = 1, 2, 3$ are Pauli matrices. The operators $\mathcal{W}_\mu = -i\partial_\mu + A_\mu(x)$, $\mu = 1, 2, 3, 4$ are hermitian. In addition to the space-time indices they contain also $SU(3)$ group indices which are suppressed in our notation.

The corresponding random matrix model is obtained by replacing \mathcal{W} by an $N \times N$ complex random matrix D that inherits the block structure and basic symmetries of the operator \mathcal{D}

$$D_4 = \begin{pmatrix} 0 & iW^\dagger \\ iW & 0 \end{pmatrix} . \quad (7)$$

The simplest candidate for the matrix W is a Gaussian random matrix generated with the probability measure

$$d\mu_4(W) = dW e^{-N\Sigma^2 \text{Tr} W^\dagger W} , \quad (8)$$

where $dW = \sum_{ij} d\text{Re}W_{ij} d\text{Im}W_{ij}$. This choice may look arbitrary at first sight but luckily it is known that the microscopic properties of the eigenvalue density of random matrices exhibit a large degree of universality which means that the microscopic density does not change for a large class of probability measures as long as they do not change the symmetry or the nature of the noise of the random matrix or introduce strong long range correlations. For example one can rigorously prove that the microscopic eigenvalue density of any random matrix generated with a probability measure $dW \exp -N\text{Tr}V(W^\dagger W)$ for a polynomial potential V is exactly the same as for the Gaussian measure (8). The microscopic properties can be however modified by adding non-analytic terms to the potential like for instance logarithmic ones. Actually such logarithmic terms come naturally into play in QCD if one integrates out fermionic degrees of freedom. Here we will however restrict ourselves only to the quenched approximation where such terms are absent. In this case the Gaussian measure is the simplest and the best candidate. The behavior of the lowest part of the spectrum can be also modified when one replaces a square matrix W by a rectangular $N_+ \times N_-$ one, where $N_+ + N_- = 2N$. Such a modification introduces $\nu = N_+ - N_-$ right-handed zero modes to the matrix D , if $N_+ > N_-$, or $\nu = N_- - N_+$ left-handed ones, if $N_- > N_+$, imitating different topological sectors. In the trivial topological sector, which we consider here, W can be viewed as a square Gaussian complex matrix (8). The microscopic eigenvalue distribution of the matrix D (7) can be calculated analytically. The calculations [2] give the expression mentioned above in eq. (3).

Consider now three dimensions. In this case there is no chiral symmetry as we will see below but one can define a two fermion family model which imitates this symmetry. The spinors have two components in the fundamental representation. There are two independent nonequivalent sets of gamma matrices $\gamma_k = \sigma_k$ and $\gamma'_k = -\sigma_k$, where as before σ_k are Pauli matrices. One can associate a fermion family with each representation and consider a common theory for the two families. A Lagrangian for such a theory can be concisely written in terms of four component spinors [10]. It takes a very similar form to the four dimensional Lagrangian. In particular it has a $U(2)$ symmetry, which is broken by a mass term to a $U(1) \otimes U(1)$ symmetry. We thus have a situation similar to the chiral symmetry in four dimensions. The main difference is that the term with γ_4 is absent in the Lagrangian. The fermionic operator takes the form

$$\mathcal{W} = i \sum_{k=1}^3 \mathcal{W}_k \sigma_k . \quad (9)$$

So in three dimension the operator \mathcal{W} is anti-hermitian $\mathcal{W} = -\mathcal{W}^\dagger$. Thus if one constructs a matrix model one should substitute a complex matrix W by an anti-hermitian one. Let us write $W = iB$

$$D_3 = \begin{pmatrix} 0 & iW \\ iW^\dagger & 0 \end{pmatrix} = \begin{pmatrix} 0 & -B \\ B & 0 \end{pmatrix} \quad (10)$$

where $B = B^\dagger$ is from a GUE ensemble with the standard measure

$$d\mu_3(B) = dB e^{-\frac{N\Sigma^2}{2} \text{Tr} B^2} , \quad (11)$$

and where $dB = \prod_{ii} dB_{ii} \prod_{i < j} d\text{Re}B_{ij} d\text{Im}B_{ij}$ is a flat measure in the set of hermitian matrices. As for D_4 (7) the eigenvalues of the matrix D_3 are purely imaginary. They also come in pairs $\pm i\lambda$. The microscopic eigenvalue density

is however different. It is given by the expression (4), so it has neither a dip nor a wavy structure. This shape just results from blowing up the central region of the Wigner semicircle eigenvalue distribution of the matrix B which is flat and has no hard edge at $\lambda = 0$. One expects that the fermionic operator of QCD₃ should reproduce this structure in the continuum limit. So we have to understand the eigenvalue density observed for staggered fermions for quenched QCD₃ shown in figure 1.

Staggered fermions

Staggered fermions discretization and its relation to continuum physics in even dimensions was discussed in [11] and in odd dimensions in [12]. Let us shortly discuss how to calculate of the spectrum of the staggered fermion operator in quenched simulations of lattice QCD. In our simulations we used the standard Wilson action to generate gauge fields

$$S_W = \beta \sum_x \sum_{\{\mu, \nu\}} \left(1 - \frac{1}{3} \text{ReTr} U_\mu(x) U_\nu(x + \mu) U_\mu^\dagger(x + \mu + \nu) U_\nu^\dagger(x + \nu) \right). \quad (12)$$

where $U_\mu(x)$ is a $SU(3)$ matrix – a dynamical variable associated with a link going between two neighboring sites x and $x + \mu$. The first sum runs over all lattice sites x , the second one over all pairs of directions $1 \leq \mu < \nu \leq D$, so S_W collects contributions from all elementary plaquettes. In the quenched approximation one generates gauge field configurations with the probability measure $\prod dU e^{-S_W}$ which is independent of fermionic degrees of freedom. One uses these configurations to compute quantum averages. In other words the influence of fermions on gauge fields is neglected in this approximation.

The staggered fermion operator is defined as [3]

$$D_{xy}^{ij} = \sum_{\mu=0}^d \eta_\mu(x) (U_\mu^{ij}(x) \delta_{y, x+\mu} - (U_\mu^\dagger)^{ij}_\mu(x - \mu) \delta_{y, x+\mu}) \quad (13)$$

where ij are indices of the $SU(3)$ matrix and $\eta_\mu(x) = (-1)^{x_1 + \dots + x_{\mu-1}}$ for $\mu = 1, \dots, D$. One can also define a parity operator $\epsilon(x) = (-1)^{x_1 + \dots + x_D}$, if the lattice has even number of sites in each direction, that divides sites into odd and even ones and introduces a chessboard structure. Each odd site has even neighbors and vice versa, so the staggered fermion matrix can be decomposed into blocks

$$D = \begin{pmatrix} 0 & D_{eo} \\ D_{oe} & 0 \end{pmatrix} \quad (14)$$

which are mutually anti-conjugated $D_{eo} = -D_{oe}^\dagger$ by construction (13). Writing $D_{oe} = iW$, one obtains a matrix of the form (10). Figure 1 tells us that the $D_{eo} = iW$ behaves for $\beta = 6.0$ as if W belonged to the universality class of Gaussian complex matrices. Since the even-odd split $D_{eo} = -D_{oe}^\dagger$ is built into the discretization scheme one can expect that the related microscopic universality is robust unless something dramatic happens that changes the basic symmetry or the nature of the randomness of the matrix. An example of such a mechanism may be a freeze-out of some degrees of freedom of the matrix.

In fact, it has been shown that in the continuum limit the staggered fermions in three dimensions corresponds to four two component spinors with the action

$$S_F = \sum_{y,k} [\bar{u}(\sigma_k \otimes I) D_\mu u - \bar{d}(\sigma_k \otimes I) D_\mu d] \quad (15)$$

where I is a two by two unit matrix. This can be equivalently written as two copies of the four component fermions defined above. Thus we expect that in the continuum limit, that is for $\beta \rightarrow \infty$, the matrix W becomes anti-hermitian, or equivalently that the fluctuations of hermitian degrees of freedom are suppressed in this limit. In the next section we propose a random matrix model describing such a gradual suppression. This model has one parameter which interpolates between the regime where W is a generic random complex matrix (with both the hermitian and anti-hermitian sectors) and the regime where it is an anti-hermitian one $W = -W^\dagger$. As it is shown below the model captures the pattern of evolution with β of the microscopic density observed in the numerical QCD₃ simulations.

Freeze-out random matrix model

The idea is to consider a random complex matrix W which is a linear combination $W = xA + iyB$ of two independent identically distributed Gaussian hermitian matrices $A = A^\dagger$ and $B = B^\dagger$ with real coefficient x, y . The matrices are generated with the probability measure

$$d\mu(A, B) = dA dB e^{-\frac{N\Sigma^2}{2}\text{Tr}A^2} e^{-\frac{N\Sigma^2}{2}\text{Tr}B^2}, \quad (16)$$

where dA and dB are flat measures for hermitian matrices. To avoid redundancy with the width parameter Σ it is convenient to restrict x, y to $x^2 + y^2 = 1$ or equivalently to parametrize $x = \cos(\alpha)$, $y = \sin(\alpha)$. We obtain a one-parameter family of matrices

$$D_\alpha = \begin{pmatrix} 0 & iW^\dagger \\ iW & 0 \end{pmatrix} = \begin{pmatrix} 0 & i\cos(\alpha)A - \sin(\alpha)B \\ i\cos(\alpha)A + \sin(\alpha)B & 0 \end{pmatrix}, \quad (17)$$

with a mixing parameter α which interpolates between (7) and (10). For $\alpha = \pi/4$ this matrix is equivalent to (7) where $W = (A + iB)/\sqrt{2}$ (8). The integration measure for W can be derived by changing variables in (16) which gives:

$$d\mu(W) \sim dW e^{-N\Sigma^2\text{Tr}WW^\dagger} \quad (18)$$

This is a standard Girko-Ginibre ensemble [13, 14]. Eigenvalues of W are uniformly distributed in a disk of radius $1/\Sigma$ in complex plane centered around the origin. For arbitrary α it becomes an elliptic ensemble with a measure

$$d\mu(W) \sim DW e^{-\frac{N\Sigma^2}{(1-\tau^2)}\text{Tr}(WW^\dagger - \frac{\tau}{2}(WW + W^\dagger W^\dagger))} \quad (19)$$

where $\tau = \cos(2\alpha)$ [15]. Eigenvalues are now uniformly distributed in an elliptic disc with semi-axes of relative length $(1 - \tau)/(1 + \tau)$. When α approaches $\pi/2$, hermitian degrees of freedom are gradually suppressed. For $\alpha = \pi/2$, W becomes purely anti-hermitian (10) and the ellipse reduces to a cut on the real axis. The evolution of the eigenvalue spectrum of the matrix D_α for α from $\pi/4$ to $\pi/2$ (or equivalently τ from 0 to -1) smoothly interpolates between the limiting eigenvalue densities $\rho_{4*}(\lambda)$ and $\rho_{3*}(\lambda)$ when α .

It is instructive to begin the analysis of the spectrum of the matrix D_α by considering the case $N = 1$. Although it is a very simplified version of the full model it allows one to understand the nature of the hard edge of the spectrum and the mechanism of its disappearance for $\alpha \rightarrow \pi/2$. For $N = 1$ the matrices A, B reduce to real numbers a, b which are independent, identically distributed normal random variables with the variance $1/\Sigma^2$. The matrix (17) has only one pair of eigenvalues

$$\lambda_\pm = \pm ir = \pm i\sqrt{a^2 \cos^2(\alpha) + b^2 \sin^2(\alpha)}. \quad (20)$$

We are now interested in finding the probability distribution of the random variable r which is constructed from a and b . This quantity has a geometrical interpretation. The vector $\vec{r} = (\cos(\alpha)a, \sin(\alpha)b)$ can be viewed as a random vector on a plane whose components are independent Gaussian variables with the standard deviations $\Sigma^{-1}\cos(\alpha)$ and $\Sigma^{-1}\sin(\alpha)$. The length of this vectors is equal to r (20). The probability distribution for this vector is an elliptic Gaussian (lines of equal probability form ellipses) so it is easy to derive the corresponding distribution of length r of the vector \vec{r} . For $\alpha = \pi/2$ the distribution reduces to a one dimensional distribution concentrated on the b -axis. In this case $r = |b|$ and thus the probability distribution of r is a half-Gaussian distribution $p(r) = 2\Sigma/\sqrt{2\pi}e^{-\Sigma^2 r^2/2}$. For $\alpha = \pi/4$ the distribution is a spherically symmetric Gaussian one and the distribution of r can be easily calculated by changing to the polar coordinates and integrating out the angle. It yields $p(r) = 2\Sigma^2 r e^{-\Sigma^2 r^2}$. For α in-between the distribution can be expressed by the following integral

$$p_\alpha(r) = \frac{\Sigma^2}{2\pi} \int_0^{2\pi} d\phi \frac{r}{\cos^2(\alpha)\cos^2(\phi) + \sin^2(\alpha)\sin^2(\phi)} \exp\left(-\frac{\Sigma^2 r^2}{2(\cos^2(\alpha)\cos^2(\phi) + \sin^2(\alpha)\sin^2(\phi))}\right) \quad (21)$$

which interpolates between the two limits. The evolution of the probability distribution with α is shown in figure 2. For small r the integral behaves as $p_\alpha(r) \sim 2\Sigma^2 r / \sin(2\alpha)$, so it goes linearly to zero with a slope $2\Sigma^2 / \sin(2\alpha)$. The slope becomes infinite for $\alpha \rightarrow \pi/2$. In this limit also the position of the maximum goes to zero and the dip gets narrower. It disappears completely only for $\alpha = \pi/2$. To summarize, we see that as long as $\alpha \neq \pi/2$ there is a repulsion from the hard edge at the origin. It can be attributed to the two-dimensional nature of the underlying

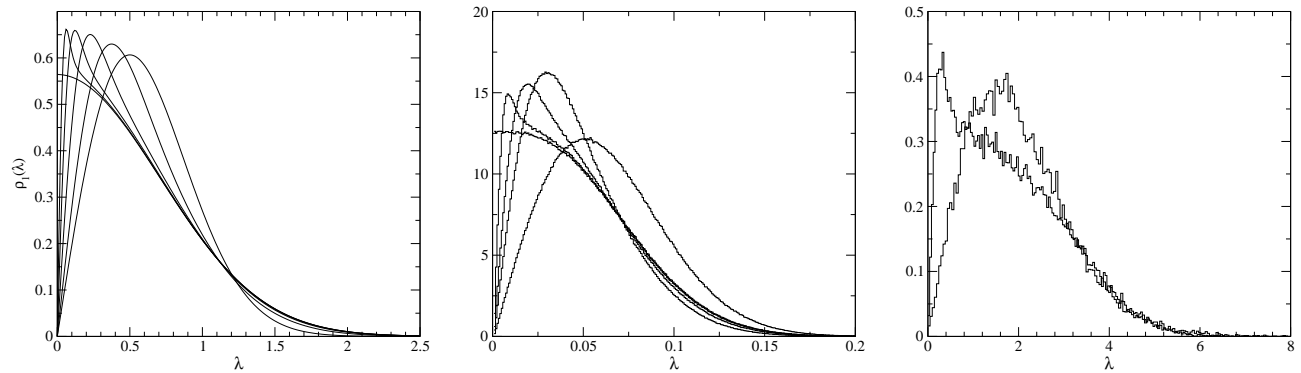


FIG. 2: The distribution $\rho_1(\lambda)$ of the lowest eigenvalue for the systems considered in this article. (Left) The distribution (21) $p_\alpha(r)$ for $\cot(\alpha) = 1.0, 0.4, 0.2, 0.1, 0.5, 0.0$. We set $\Sigma = 1$. The maximum moves from right to left when α is decreased. The function $p_\alpha(r)$ goes linearly to zero $p_\alpha(r) \sim 2r/\sin(2\alpha)$ for $r \rightarrow 0$ with a coefficient $2/\sin(2\alpha)$. The dip disappears only for $\sin(2\alpha) = 0$. (Middle) The distribution of the lowest eigenvalue obtained numerically for the matrix D_α in the matrix model for $N = 20$ and for $\cot(\alpha) = 0.0, 0.02, 0.05, 0.10, 1.0$. As before the maximum moves from right to left when α is increased from $\pi/4$ to $\pi/2$. The linear part of the slope at zero has a coefficient which increases when α approaches $\pi/2$. (Right) QCD₃ for $\beta = 12$ and 30 on 24^3 lattices. The eigenvalues are rescaled according to (2).

distribution of the vector $(\cos(\alpha)a, \sin(\alpha)b)$ in the plane. The hard edge and the repulsion completely disappears only for $\sin(2\alpha) = 0$ where the distribution becomes one-dimensional. We expect the same mechanism of repulsion for the smallest eigenvalue of the matrix D_α (17) also for $N > 1$. As long as both hermitian and anti-hermitian degrees of freedom are active the lowest eigenvalues will be repelled from zero. Indeed we see in figure 2 in the middle that the evolution of the probability density for the lowest eigenvalue of the matrix D_α for $N = 20$ very much resembles that shown in the left panel. For large α the distribution has a shape of the type $re^{-r^2/2}$, while for small ones it is more like a semi-Gaussian shape with an additional narrow peak on top of it. This additional peak gets narrower when $\alpha \rightarrow \pi/2$ and it moves towards zero. The same pattern is observed also for larger N . Finally, in the right chart we show corresponding plots in QCD₃ data.

The repulsion has also an influence on the second smallest eigenvalue, the third smallest one etc. For $\alpha \rightarrow \pi/2$ the repulsion range becomes smaller and correspondingly the influence on higher eigenvalues becomes smaller too. The resulting microscopic eigenvalue distribution will be discussed in the next section where it will be compared to the corresponding histograms for quenched QCD₃ for different values of β .

Comparison of QCD₃ to the random matrix model

In figure 3 we show histograms of eigenvalue distribution for QCD₃ for different values of $\beta = 6.0; 12.0; 18.0$ for 24^3 lattice (lhs) and for the matrix model (5) for different values of $\cot(\alpha) = 1.0; 0.1; 0.05$ and $N = 100$ (rhs). When β and α decrease the wavy structure gradually disappears in a very similar way in both cases as one can see by comparing the figures. One should notice an anomaly in the plot in the bottom-left panel for $\beta = 18.0$ where the main peak seems to be slightly wider than the corresponding peaks in other panels. The broadening is related to an effect of eigenvalue pairing which appears when β is increased. The pairing means that the distance between the first and the second eigenvalue, the third and the fourth one, etc decreases when β increases. For $\beta = 18.0$ the distribution of the first one and the second one are so close to each other, as shown in figure 4, that they contribute to one broader peak in the eigenvalue density function seen in the bottom-left plot in figure 3. For $\beta \rightarrow \infty$ the distance between neighboring eigenvalues tends to zero giving degenerate pairs of eigenvalues in the limit as one can see in the right chart in figure 4. This is in agreement with what one expects from the continuum theory (15) for which the Dirac operator indeed has doubly degenerate eigenvalues.

Summary and discussion

We showed that a simple two-matrix model reproduces basic characteristic features observed in the eigenvalue spectra of the Dirac operator in staggered QCD₃ data. The mixing parameter $\tau = \cos 2\alpha$ interpolates between the regime where block matrices W (19) in the Dirac matrix (17) are complex to the regime where they are anti-hermitian.

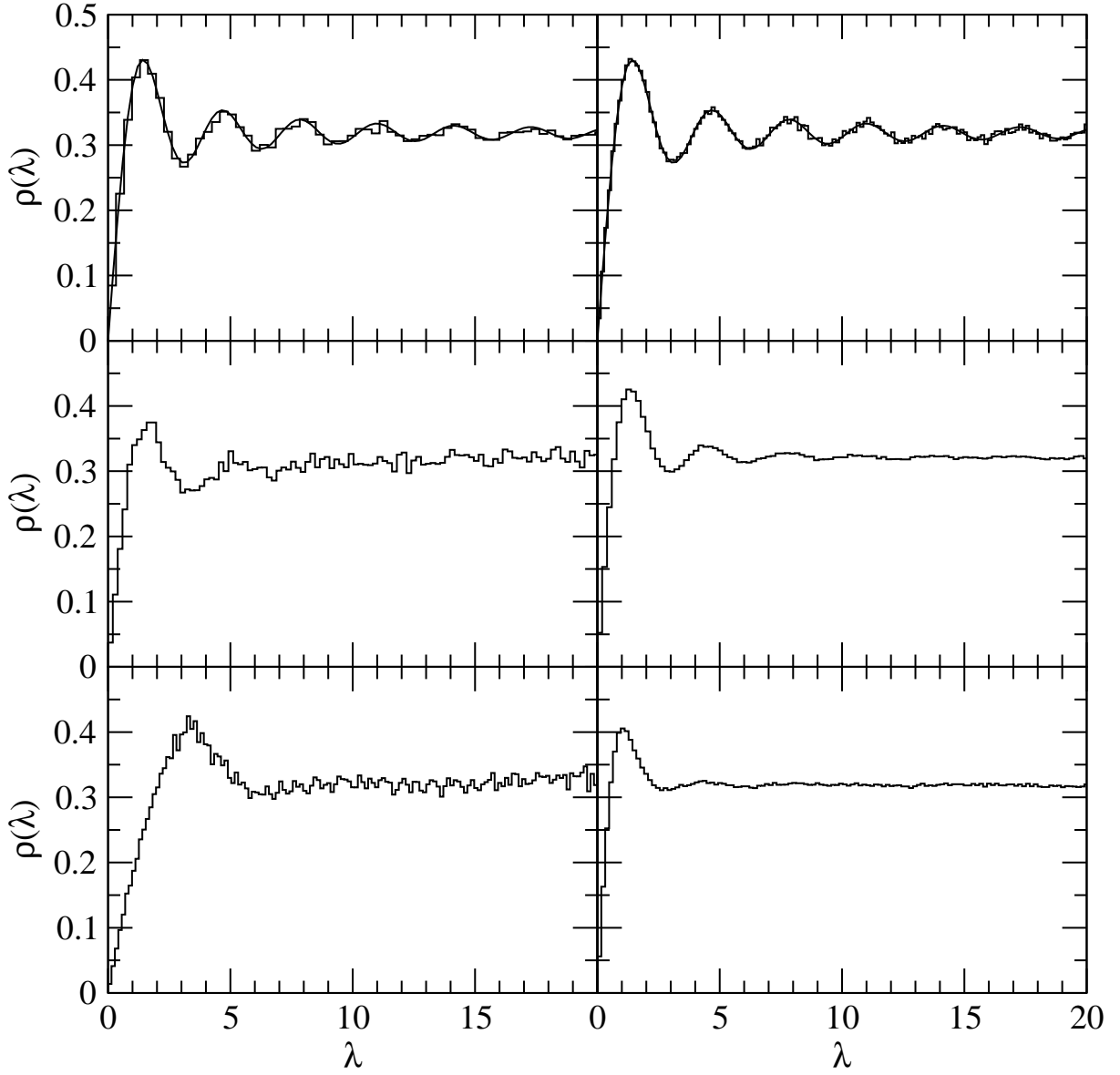


FIG. 3: Left: eigenvalue distribution for QCD₃ for $\beta = 6.0; 12.0; 18.0$ for lattices $14^3, 24^3, 24^3$ respectively. Right: eigenvalue distribution for D_α for the matrix model for $\cot(\alpha) = 1.0; 0.1$ and 0.05 for 50×50 matrices.

In the former case the microscopic density is given by (3) while in the latter one by (4). We observe a similar evolution in the QCD₃ data. The shape of the probability distribution of the lowest eigenvalue evolves in both the cases in a similar way too. The nature of finite size effects manifesting as the appearance of a small narrow peak on top of the distribution as well as the gradual disappearance of the hard core close to the origin is similar in both the cases too. What remains to show is how the microscopic density precisely interpolates between the two limiting cases (3) for $\alpha = \pi/4$ ($\tau = 0$) and (4) for $\alpha = \pi/2$ ($\tau = -1$). We expect that a continuous evolution of the microscopic density can be observed in a parameter $\hat{\alpha} = \sqrt{N}(\pi/2 - \alpha)$ in a double scaling limit, that is for $N \rightarrow \infty$, $\alpha \rightarrow \pi/2$ and for finite $\hat{\alpha}$. This limit corresponds to a very asymmetric mixing of hermitian and anti-hermitian degrees of freedom $W \approx (\hat{\alpha}/\sqrt{N})A + iB$. The width of fluctuations of hermitian degrees of freedom decreases with the system size as $1/\sqrt{N}$ and the aspect ratio τ of the elliptic ensemble (19) approaches minus one as $\tau = -1 + 4\hat{\alpha}^2/N$. The evolution of the shape with $\hat{\alpha}$ can be found using for instance the supersymmetric method [16]. Having done that one can try to relate the parameter $\hat{\alpha}$ to β in QCD₃. We leave this issue for future investigations.

Acknowledgements

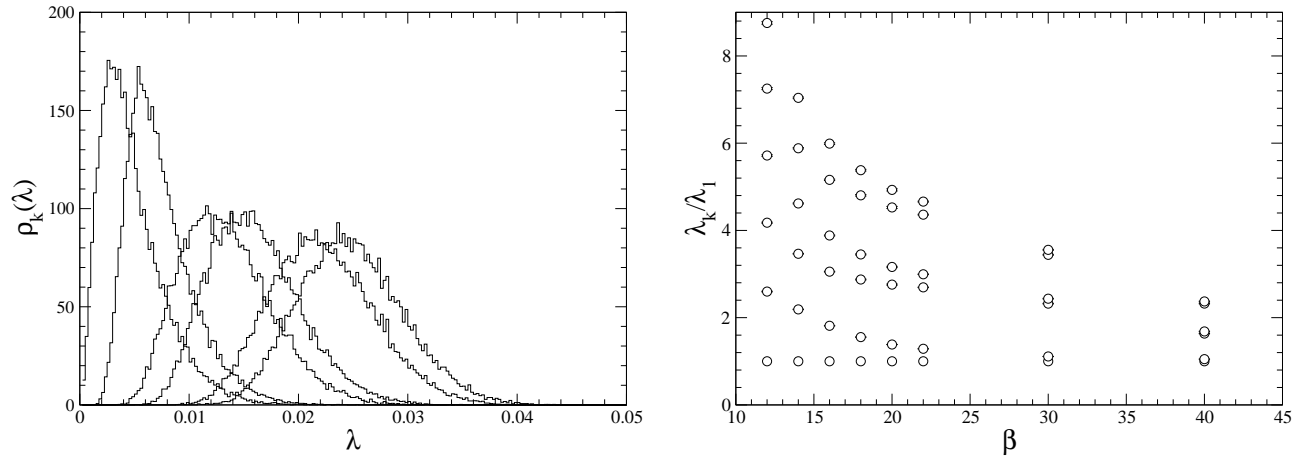


FIG. 4: (Left) Histograms of individual eigenvalues for QCD₃ with $\beta = 18.0$ on 24^3 lattice. (Right) Averages of the first six eigenvalues in QCD₃ for $N = 24^3$ as a function of β . All eigenvalues are normalized to the smallest eigenvalue for given β .

This work was supported by the EC-RTN Network “ENRAGE”, No. MRTN-CT-2004-005616 and the Polish Ministry of Science Grant No. N N202 229137 (2009-2012).

-
- [1] E.V. Shuryak, J.J.M. Verbaarschot, Nucl.Phys. **A560** 306 (1993);
 - [2] J.J.M. Verbaarschot and I. Zahed, Phys. Rev. Lett. **70**, 3852 (1993);
 - [3] T. Banks, J.B. Kogut and Susskind, Phys. Rev. **D 13** 1043 (1976); L. Susskind, Phys. Rev. **D 16** 3031 (1977);
 - [4] P.H. Damgaard, U.M. Heller and A. Krasnitz, Phys. Lett. **B445**, 366 (1999);
 - [5] E. Follana, A. Hart, C.T.H. Davies, Q. Mason, Phys. Rev. **D72** (2005) 054501.
 - [6] J.J.M. Verbaarschot and I. Zahed, Phys. Rev. Lett. **73**, 2288 (1994);
 - [7] P.H. Damgaard, U.M. Heller, A. Krasnitz and T. Madsen Phys.Lett. B440 (1998) 129;
 - [8] J.J.M. Verbaarschot and T. Wettig, Ann. Rev. Nucl. Part. Sci. **50** 343 (2000);
 - [9] J.J.M. Verbaarschot, *QCD, Chiral Random Matrix Theory and Integrability*, Les Houches lectures notes, arXiv:hep-th/0502029;
 - [10] R.D. Pisarski, Phys. Rev. **D29**, 2423 (1984);
 - [11] H. Kluberg-Stern, A. Morel, O. Napoly and B. Petersson, Nucl. Phys. **B 220** [FS8] 447 (1983);
 - [12] C. Burden and A.N. Burkitt, Europhys. Lett. **3** (5) 545 (1987);
 - [13] J.Ginibre, J. Math. Phys. **6**, 440 (1965)
 - [14] V. L. Girko, *Spectral theory of random matrices*, in Russian (Nauka, Moscow 1988), and references therein.
 - [15] H.-J. Sommers, A. Crisanti, H. Sompolinsky, and Y. Stein, Phys. Rev. Lett. **60**, 1895 (1988);
 - [16] J.J.M. Verbaarschot, *The Supersymmetric Method in Random Matrix Theory and Applications to QCD*, Lectures given at the 2004 ELAF Summer School in Mexico City arXiv:hep-th/0410211;